Photoconductivity of carbon aerogels

M. Hosoya,[a] G. Reynolds, and M. S. Dresselhaus[b]
Department of Physics, Massachusetts Institute of Technology, Cambridge, Massachusetts 02139

R. W. Pekala
Chemistry and Materials Science Department, Lawrence Livermore National Laboratory, Livermore, California 94550

(Received 5 October 1992; accepted 7 December 1992)

Photoconductivity was measured on a series of carbon aerogels to investigate their electronic properties. Carbon aerogels are a special class of low-density microcellular foams, consisting of interconnected carbon particles (~120 Å diameter) and narrow graphitic ribbons (~25 Å width) intertwined within each particle. Both the dark- and photoconductivities show drastic changes in the temperature range 5–300 K, which are similar to those in *a*-Si and chalcogenide photoconductors. At high temperatures, the photoconductivity is dominated by the carrier recombination within each particle. The photoconductivity at low temperatures is dominated by the same carrier transport mechanism as that for the dark conductivity, which is based on hopping and tunneling transport. The activation energy values for transport and recombination identify the electronic structure of the particles among samples of different bulk density. The long decay time of the photoconductivity suggests a relaxation mechanism associated with the dangling bonds.

I. INTRODUCTION

A photoinduced excess conductivity has been observed in disordered carbon materials.[1–5] These observations provide useful information for understanding the electronic properties, especially for the structural defects, the carrier transport, and the recombination. So far, photoconductivity in vapor-grown carbon fibers,[1] evaporated carbon films,[2] pyrolyzed cellophane films,[3] and activated carbon fibers (ACF)[4,5] has been reported. Kuriyama and Dresselhaus[4,5] measured the temperature dependence of the photoconductivity and its decay time in ACF's, and explained their experimental results in terms of localized states and hopping conduction. However, it was difficult to provide a quantitative description of ACF photoconductivity, because the photoconductivity did not show a dramatic change over the temperature range from 30 to 290 K.

As a class of disordered carbon materials, carbon aerogels have been under investigation with regard to their structure-property relationships.[6–12] The aerogels are cluster-assembled, low-density porous materials, consisting of interconnected carbon particles with diameters of ~120 Å. Within each particle, a glassy-carbon-like nanostructure is observed, consisting of an intertwined network of narrow graphitic ribbons of width ~25 Å. Their morphology is illustrated schematically in Fig. 1. This structure leads to extremely high surface areas (600–800 m^2/g) with a large fraction of the atoms covering the surface of the interconnected particles, so that electronic properties different from other disordered carbons are expected.

In this paper, we show the dark- and photoconductivities of the carbon aerogels and the decay time of the photoconductivity in the temperature range from 5 K to 300 K. The illumination power dependence of

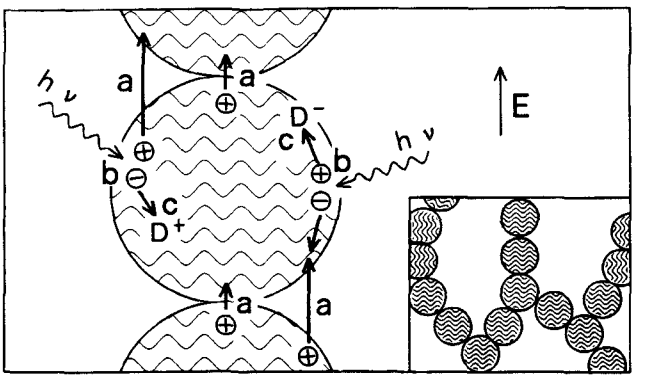

FIG. 1. Schematic diagram of the carbon aerogel morphology (inset) and electronic processes. The carrier transport by hopping and tunneling (a), the photocarrier generation (b), and the carrier recombination between the carriers and the recombination centers (c) are discussed in the text. Hopping and tunneling can also take place between ribbons in a single particle. D^+ and D^- show the dangling bonds.

[a]Present address: Toshiba R&D Center, 1, Komukai Toshiba-cho, Saiwaiku, Kawasaki 210, Japan.
[b]Also with Department of Electrical Engineering and Computer Science, Massachusetts Institute of Technology, Cambridge, Massachusetts 02139.

 © 1993 Materials Research Society

https://doi.org/10.1557/JMR.1993.0811 Published online by Cambridge University Press

the photoconductivity and both the recombination and transport kinetics are also investigated. The results show drastic variations of both the dark- and photoconductivities in this temperature range. The photoconductivity shows similar trends as that in *a*-Si and chalcogenide photoconductors. Quantitative analysis reveals insight into the transport and recombination mechanisms.

II. EXPERIMENTAL DETAILS

The carbon aerogels used in this study are derived from the sol-gel polymerization of resorcinol powder and formaldehyde, with sodium carbonate as the base catalyst.[6,7,9–11] The (Resorcinol)/(Catalyst) (R/C) ratio dominates the particle size, surface area, and mechanical properties of the carbon aerogels. In this experiment, all samples were synthesized at R/C = 200, and the aerogel density was controlled by varying the reactant concentration of the starting solution. Upon completion of the cure cycle (20–95 °C), the cross-linked Resorcinol-Formaldehyde (RF) gels were washed with fresh acetone and then placed in a jacketed pressure vessel filled with liquid carbon dioxide. After flushing the acetone from the pores of the gel, the vessel was heated above the critical point of carbon dioxide (T_c = 31 °C, P_c = 7.4 MPa). The resultant RF aerogels were subsequently pyrolyzed at 1050 °C in a nitrogen atmosphere to form carbon aerogels.

A carbon aerogel sample of 9 mm × 5 mm × 4 mm in size, with properties listed in Table I, was mounted on a mica substrate that was set on an oxygen-free copper heat sink. The heat sink was suspended in a continuous-flow cryostat, consisting of a liquid nitrogen outer bath and a liquid helium inner bath. The sample was cooled by a flow of cold helium gas controlled by a throttle valve. The temperature was controlled from 4.2 K to 300 K by a temperature controller unit connected to a heater and a thermocouple mounted on the heat sink. Electrical contact to the sample was made with silver paint, and four copper wires were attached, as shown in Fig. 2. A dc four-terminal method was used for the conductivity measurements with a constant 100 μA current source. The potential difference V between inner electrodes was measured by a nanovolt meter, while a constant current I was flowing between the outer

TABLE I. Properties of carbon aerogel samples with different densities.

Density (g/cm^3)	0.118	0.449	0.646
R/C ratio		200	
Particle diameter (Å)[12]		120 ± 15	
L_a (Å)[12]	29	26	27
Conductivity at 300 K (Ω^{-1} cm^{-1})	0.85	8.1	22

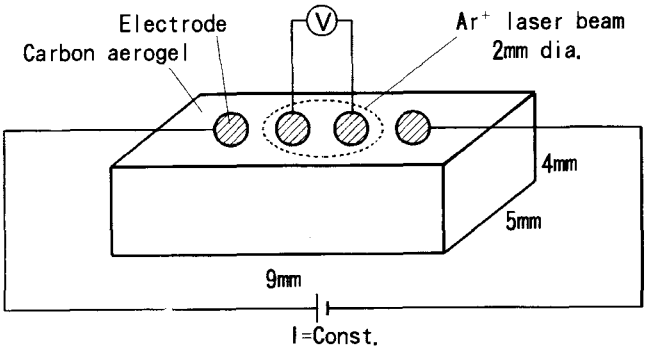

FIG. 2. Geometry of the carbon aerogel sample and the electrodes. The sample is mounted on a mica substrate, set on a copper heat sink that is suspended in a continuous-flow cryostat.

electrodes. The conductivity was calculated by

$$\sigma = \frac{1}{2\pi s}\frac{I}{V} \quad (1)$$

where s is the distance between the electrodes, equal to 1 mm in this experiment.

In the photoconductivity measurements, an Ar ion laser beam (488 nm wavelength) with a 2 mm spot size was focused onto the center of the sample surface through a quartz window. As shown in Fig. 2, the beam covered the two inner electrodes. In order to diminish the heating effect by the laser illumination to a negligible level, the surface temperature of the sample during the illumination was measured by attaching a thermocouple just beside the illuminating position. Because the temperature measured by the thermocouple started to rise when the illuminating power at the sample surface exceeded 10 mW, 1 mW was selected as the standard illuminating power in the present work.

To diminish the heating effect further, we also measured the ac photoconductance using an optical chopper with a 20% duty cycle, and operating at a frequency of 10 Hz and using a lock-in amplifier. In this measurement, the constant 100 μA current source was connected to the inner electrodes and the potential difference between the same inner electrodes was measured during the chopped illumination. This two-probe method was used because the signal was too small to be measured with the four-terminal method used for the dc measurements described above. Therefore, we could measure only ac photoconductances, rather than ac photoconductivities, in this experiment.

The decay time of the photoconductivity was measured to discuss the carrier recombination kinetics. The laser illumination was continued until a steady photocurrent was obtained, and then the decay of the photocurrent was observed in the dark with an oscilloscope. We define the decay time as the time period in which the photocurrent decreases to 50% of the steady photocurrent.

https://doi.org/10.1557/JMR.1993.0811 Published online by Cambridge University Press

III. RESULTS AND DISCUSSION

A. Dark conductivity

The temperature dependence of the dark conductivity for the three samples is shown in Fig. 3 on a semi-log plot of log σ vs temperature. The conductivity increases as the density of the sample increases. This result is attributed to the morphology of the carbon aerogels. With increasing density at constant (Resorcinol)/(Catalyst) ratio, the colloidal-like particles which are loosely connected at low density now become more closely packed, forming a highly linked network to cause easier carrier transport among the particles. Of particular interest is the sharp decrease in conductivity σ at low temperatures below 30 K. Especially, the least dense sample shows a striking decrease in σ of about six orders of magnitude. This strong temperature dependence is attributed to some form of hopping conduction mechanism or tunneling behavior.

For the purpose of investigating the dark conduction mechanism, we have fit the data, based on the fluctuation induced tunneling (FIT) model.[13] Fung *et al.*[12] tried to fit the electrical conductivity with various conduction models, including nearest-neighbor hopping, variable range hopping, and charge-energy-limited-tunneling, and found a good fit for their data to the FIT model. The FIT model was proposed by Sheng *et al.*[13] to explain the conduction mechanism for carbon-PVC composites, consisting of conductive carbon particles of 140–350 Å in diameter, embedded in an insulating PVC matrix. These materials are composed of a network of touching or nearly touching graphitic spheres, so that there are many similarities between these materials and our carbon aerogel materials.

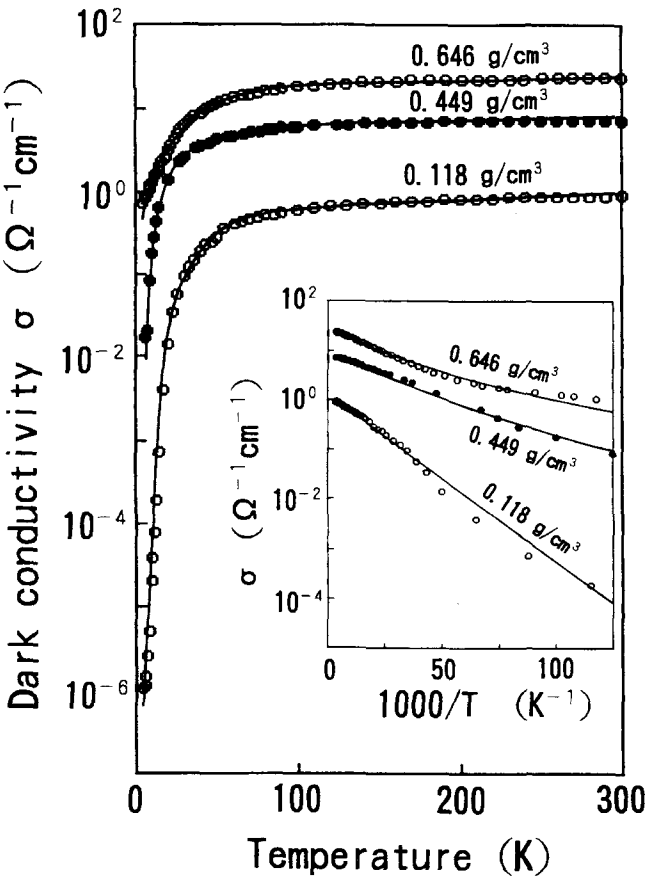

FIG. 3. The temperature dependence of the dark electrical conductivity for carbon aerogels of three densities. The solid lines show the fit of the fluctuation-induced tunneling (FIT) model. The inset indicates the plots against $1000/T$. The fitting values are listed in Table II.

In the FIT model, it is assumed that the tunneling current of electrons through the potential barriers between carbon particles is driven by thermally activated voltage fluctuations across the barrier. Under a weak external field, the fluctuations give rise to a tunneling current and the following expression for the temperature dependence of the conductivity was obtained:

$$\sigma = \sigma_0 \exp\left(-\frac{T_1}{T + T_0}\right). \tag{2}$$

Here, σ_0 is a pre-exponential factor which is treated as a constant, and T_0 and T_1 are characteristic temperatures. Equation (2) states that at low temperatures ($T < T_0$) the conductivity is temperature independent and reduces to the form $\sigma_0 \exp(-T_1/T_0)$ for tunneling through a parabolic barrier. In contrast, at high temperatures the behavior becomes that of thermal activation with an activation energy kT_1, where k is Boltzmann's constant, and σ approaches σ_0 at very high T.

The fit of the model is shown by the solid curves in Fig. 3. The fitting values are listed in Table II. The values of the ratio (T_1/T_0) increase drastically as the density decreases, which shows that the tunneling probability for the least dense aerogel is extremely small compared with that of high density samples at low temperatures. This result is considered to be due to the increasing size of the mesopores between particle chains (see Fig. 1) and the resulting poor electrical interconnectivity of the particles in the carbon aerogels of the lowest density. Also of interest are the values of the thermal activation energy, kT_1, which are found from the log σ vs $1/T$ plots in the inset, yielding values in the range of 4.0–6.7 meV, as shown in Table II. At high temperatures, the thermal

TABLE II. Values for the fitting parameters used in the fluctuation-induced tunneling conduction model and for the estimated activation energy (kT_1).

Density (g/cm³)	0.118	0.449	0.646
σ_0 ($\Omega^{-1} \cdot cm^{-1}$)	1.1	9.3	28
T_1 (K)	78	48	46.7
kT_1 (meV)	6.7	4.1	4.0
T_0 (K)	0.1	2.4	4.2

https://doi.org/10.1557/JMR.1993.0811 Published online by Cambridge University Press

activation over the potential barrier, rather than the tunneling through the barrier, dominates the conduction process. The result that the activation energy is least for the most dense sample is consistent with the results for (T_1/T_0).

Although a good fit was obtained for the dark conductivity with the FIT model, there might be other transport models that also fit the data because the carbon aerogels involve disorder, consisting of pores and particles. We will next consider the photoconductivity results to investigate the conduction mechanism more precisely.

B. Photoconductivity

Figure 4 shows experimental results for the temperature dependence of the dc-photoconductivity, which is observed to increase with increasing density. This is due to the larger photon absorption per unit volume, because of the denser packing of particles, and the higher tunneling probability in the higher density samples. Starting at 5 K, the photoconductivity first increases with increasing temperature, and reaches a peak at ~20 K, above which $\Delta\sigma$ decreases. This decrease can be attributed to a decrease in the photocarrier density due to the fast recombination of the photocarriers with thermally activated dark carriers. On the other hand, the increase in photoconductivity with increasing temperature below 20 K implies that the transport of the photocarriers is limited by the same mechanism as that for the dark carriers, and that the photocarrier mobility is thermally activated.

The ratio $\Delta\sigma/\sigma$ is shown in Fig. 5, where $\Delta\sigma$ is the photoconductivity and σ is the dark conductivity. The ratio $\Delta\sigma/\sigma$ decreases monotonically with increasing temperature, and the density dependence of $\Delta\sigma/\sigma$ is rather small, compared with that of $\Delta\sigma$ and σ, individually. Of interest is the observation that at temperatures where $\Delta\sigma$ gives the maximum value in Fig. 4, the three samples show approximately the same $\Delta\sigma/\sigma$ value of ~0.2. This result implies that the photocarrier population starts decreasing with increasing temperature when the population of the thermally excited dark carriers exceeds five times that of the photocarriers. In contrast, at low temperatures (<20 K), the population of thermally activated dark carriers decreases, causing a larger difference in $\Delta\sigma/\sigma$ among the three samples.

To discuss the photoconductivity more precisely, the data are plotted against $1000/T$ in Fig. 6, with the dark conductivity drawn by solid lines. The dark conductivity

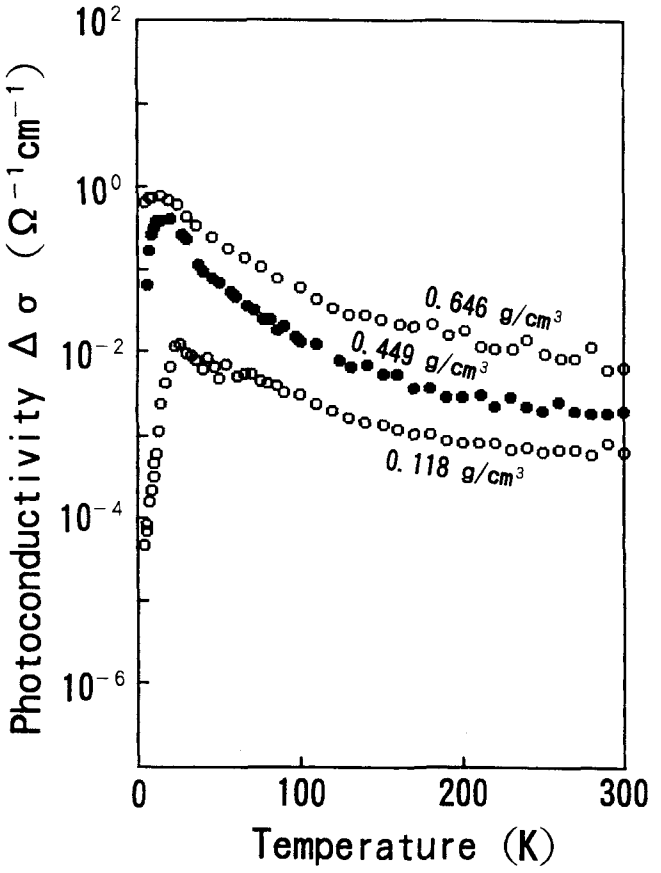

FIG. 4. The temperature dependence of the dc-photoconductivity for the three carbon aerogel samples.

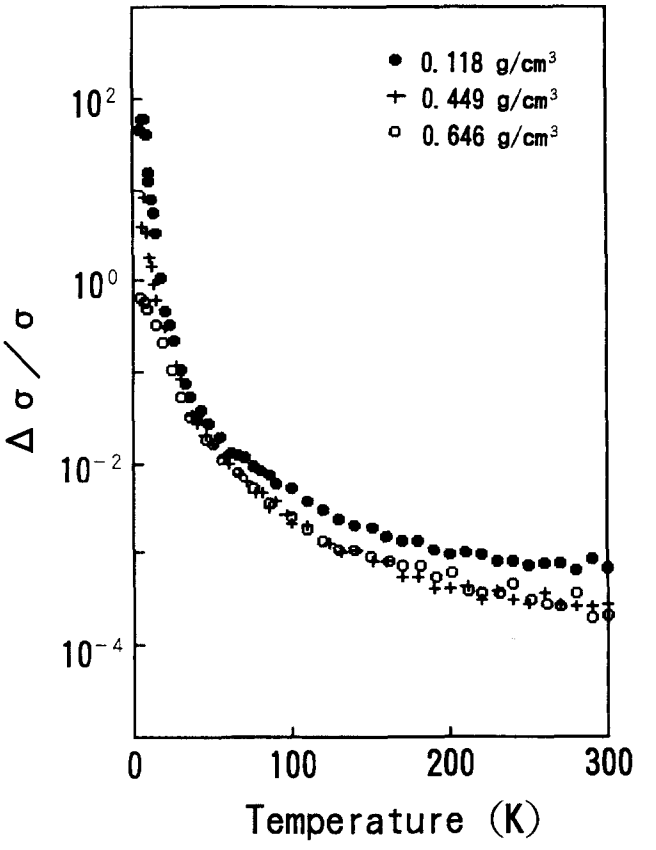

FIG. 5. The temperature dependence of the ratio (photoconductivity $\Delta\sigma$)/(dark conductivity σ) for carbon aerogel samples with three different densities.

https://doi.org/10.1557/JMR.1993.0811 Published online by Cambridge University Press

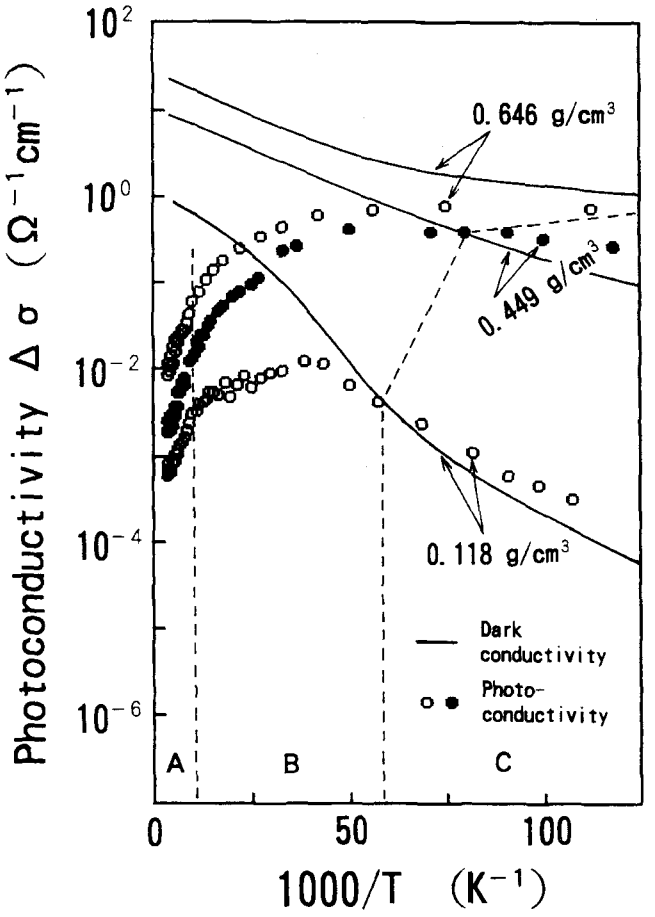

FIG. 6. The photoconductivity plotted against $1000/T$. In the high temperature range A, carrier recombination dominates the photoconductivity. In contrast, it exerts minor effects on $\Delta\sigma$ in the low temperature range C (see text).

and photoconductivities cross at temperatures near the peaks of the photoconductivity, and the photoconductivity shows a linear dependence on $1000/T$ in the high and low temperature ranges, that is, in ranges A and C. Exactly the same tendencies were reported in the photoconductivity of a-Si[14,15] and the calcogenides,[16] although their peaks appear in the higher temperature ranges of ~250 K to ~400 K. This discrepancy in the temperature T_{max} can be attributed to the difference in the ratio $\Delta\sigma/\sigma$, because a-Si and the calcogenides are much more efficient photoconductors, showing high $\Delta\sigma/\sigma$ values even at high temperatures. This interpretation is consistent with our results, where the least dense sample with the highest $\Delta\sigma/\sigma$ value shows the highest T_{max} among the three samples.

In the high temperature range A in Fig. 6, carrier recombination dominates the photoconductivity, because the dark carrier population is much larger than that of the photocarriers. In the steady state, the photocarrier generation rate G is equal to the recombination rate. Therefore, we obtain the following equations, using the activation energy E_r for the recombination, the recombination constant K, the photocarrier density Δn, the density of the recombination centers N, the Boltzmann constant k, the electron charge magnitude e, and the mobility μ of the photocarriers:

$$\Delta\sigma = \Delta n e \mu \tag{3}$$

$$G = K\Delta n N \exp(-E_r/kT) \tag{4}$$

From Eqs. (3) and (4), we find that

$$\Delta\sigma = \frac{eG\mu}{NK} \exp(E_r/kT) \tag{5}$$

The fits to Eq. (5), shown in the inset of Fig. 7, give almost the same activation energies (22–25 meV) for the three samples, independent of the density of the carbon aerogel (Table III). This indicates that recombination takes place within the particles and that the electronic structures within the particles are identical among these three samples. Another indication for the existence of recombination centers within the particles is the larger activation energies for the recombination (22–25 meV) as given in Table III relative to those for the dark conductivity (4–7 meV) shown in Table II. This result is consistent with the long decay time photoconductivity discussed below, because the high activation energies cause low recombination probabilities.

In the low temperature range C in Fig. 6, the population of the photocarriers is larger than that of the dark carriers. Therefore, we can estimate the activation energy E_t for the transport by fitting the low temperature data for the least dense sample to

$$\Delta\sigma = \Delta\sigma_0 \exp(-E_t/kT), \tag{6}$$

and yielding $E_t = 5.7$ meV for the least dense sample, as shown in Fig. 7 and listed in Table III. This value is close to the activation energy for the dark conductivity (6.7 meV) shown in Table II, which is consistent with having the same transport mechanism for the photoconductivity as that for the dark conductivity. Therefore, at low temperatures $\Delta\sigma$ is dominated by the hopping and tunneling of carriers between the particles. In contrast, the carrier recombinations exert minor effects on $\Delta\sigma$, but are responsible for the longer decay time.

The above results are consistent with the data of the thermally activated decay time shown in Fig. 8. At low temperatures, the decay time shows sharp decreases with increasing temperature, which is attributed to the increase of the dark carrier population. Of particular interest is the extremely long decay times below ~40 K, especially for the lowest density aerogel (22 s at 5 K). Long decay times of the photoconductivity in disordered carbons were reported previously.[1–5] They were measured in previous work at $T > 30$ K, and the decay times were in the range from 50 ms to several seconds.

https://doi.org/10.1557/JMR.1993.0811 Published online by Cambridge University Press

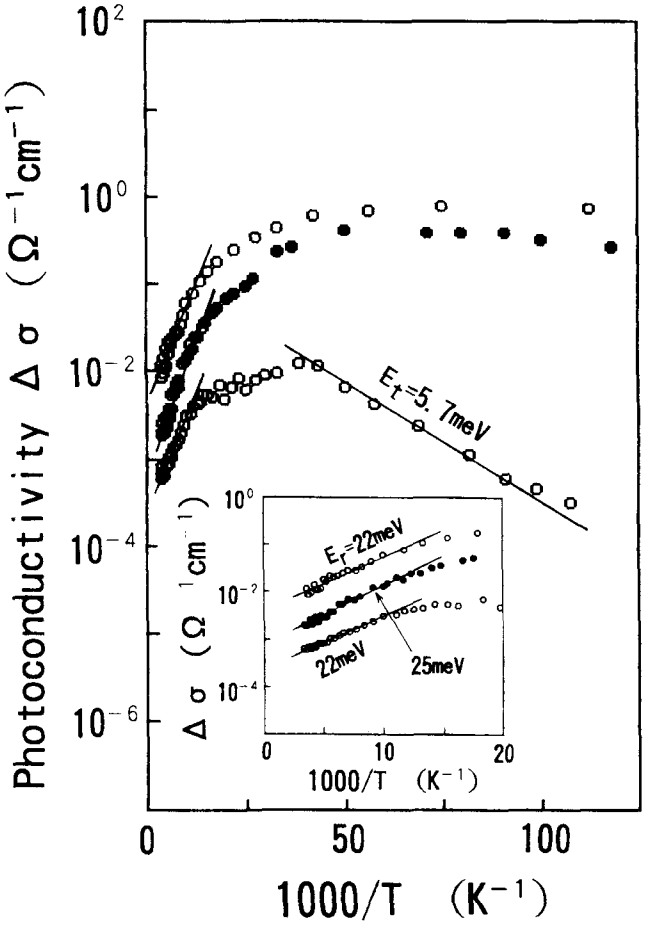

FIG. 7. The fit for the photoconductivity $\Delta\sigma(T)$ and the estimated activation energies for the carrier recombination in range A and for the hopping in range C, following the notation of Fig. 6. The inset provides an expanded scale for the high temperature data.

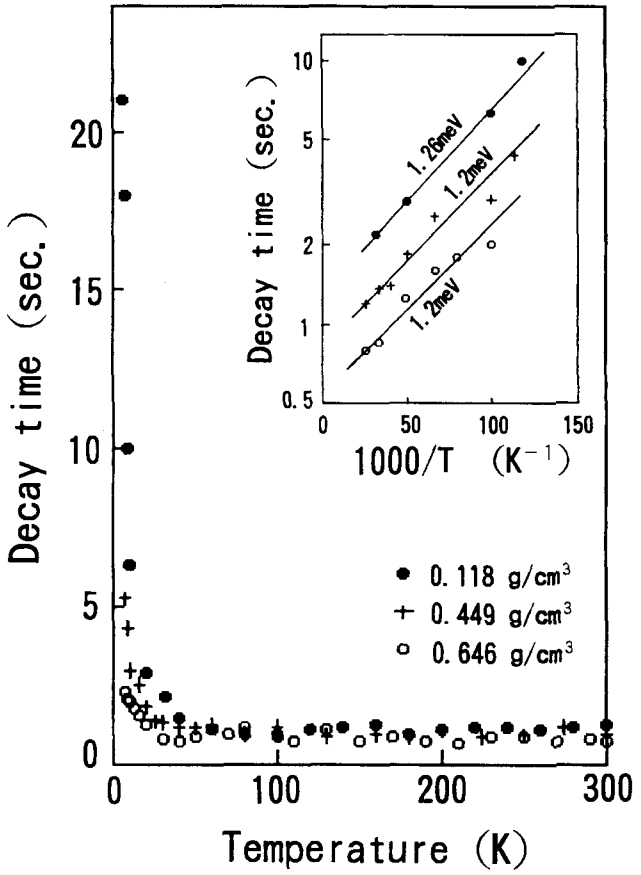

FIG. 8. The temperature dependence of the decay time in the carbon aerogels. The activation energies for the decay time are shown in the semilog plot in the inset.

Our results, showing extremely long decay times below 40 K, are also similar to the decay-time behavior for persistent photoconductivity (PPC) in GaAs[17,18] and *a*-Si:H,[19,20] which show decay times of seconds to weeks. In these materials, the long decay time is explained by a polaronic state of the photocarriers hopping between the dangling bonds. The hopping gives rise to charged dangling bonds, but they are screened by the surrounding bond relaxations, facilitated by the flexible surface microstructure. The screened photocarriers behave like neutral particles and their recombination is remarkably reduced, thus causing long decay times.

The associated activation energies below 50 K for the carbon aerogels are estimated to be in the range 1.20–1.26 meV from the inset of Fig. 8. These activation energies are also almost independent of the sample density, indicating that the recombinations take place within each particle. These values for the activation energy are much smaller than those obtained for the high temperature range from Fig. 7. This can be attributed to smaller bond relaxation and weaker screening at low temperatures because of the lower carrier mobility. Although the activation energies are smaller at low temperature, the longer decay times can be observed because the population of the dark carriers shows a sharper decrease than the decrease in the activation energy.

Other information on the recombination kinetics is provided in Fig. 9, which shows a log-log plot of the photoconductivity versus illumination power, with the gradients of the curves indicated in the figure. At 300 K, all curves have a gradient of unity, which implies a monomolecular recombination process. Monomolecular recombination is generally observed when the density of photocarriers is much smaller than that of the dark carriers.[21,22] This result is consistent with Fig. 5, where the magnitude of the photoconductivity is shown to be lower than 0.1% of the corresponding dark conductivity. In contrast, at low temperatures the slow recombination restricted by the energy barrier results in a higher photocarrier density. When the photocarrier density is high enough to neglect the dark carrier density, the recombination takes place among the photocarriers independently of the dark carrier density. Thus, the medium

https://doi.org/10.1557/JMR.1993.0811 Published online by Cambridge University Press

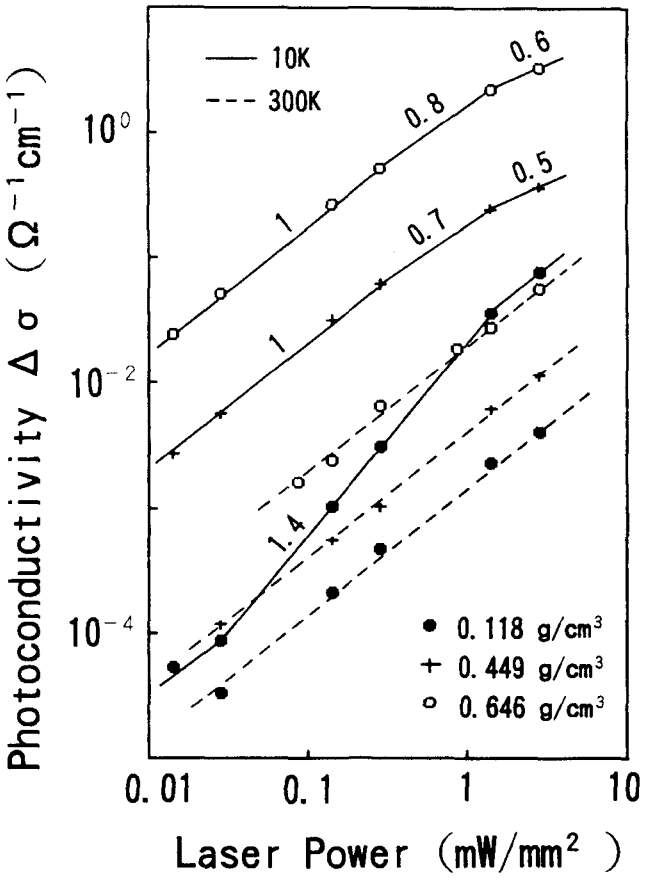

FIG. 9. The laser-power dependence of the photoconductivity at 10 K and 300 K. The recombination kinetics are indicated by the gradients of the curves (see text).

density aerogel shows bimolecular recombination in the high illumination power region at 10 K, as shown by solid lines in Fig. 9. This is also consistent with Fig. 4, because in the range of 1.8–3.5 mW/m^2, where the middle density sample shows the bimolecular process, the ratio $\Delta\sigma/\sigma$ is supposed to be larger than 10. In other regimes for the two higher density samples, a mixture of bimolecular and monomolecular recombination processes is observed.

It should be noticed in Fig. 9 that at 10 K the least dense aerogel shows a supralinearity in the illuminating power range of 0.035–1.8 mW/mm^2, where the gradient is 1.4. Supralinearity in other materials such as CdS was previously reported,[23,24] and is understood to be caused by the "electronic doping" from one class of recombination centers to another. Suppose one set of recombination centers captures holes under photoexcitation, and, as a result, electrons which were in the above recombination centers transfer into another set of recombination centers. If the first set of recombination centers has a low electron capture cross section, the probability of the recombination of photogenerated electrons becomes extremely low, resulting in a high photoelectron density and supralinearity. After all the recombination centers of the first set capture holes, the photoconductivity again increases linearly with illuminating intensity. Since this phenomenon is frequently observed over a short range of rather low illuminating intensities in a good photoconductor such as CdS, it is considered to be reasonable to observe the supralinearity in the least dense carbon aerogel sample at low temperature range, where the photocarrier population is much larger than that of the dark carriers. In this context, it is assumed that there are at least two classes of recombination centers in the carbon aerogel. The existence of these two classes of recombination centers can be attributed to the geometry of the aerogel, since it involves two classes of dimensions, that is, the carbon particles of 120 Å in size and the nanostructure within each particle consisting of an intertwined network of narrow graphitic ribbons with a width of ~25 Å. Thus, there may be two classes of recombination centers; one of which exists at the surface of the particles and another within the particles.

We note that the contribution of a heating effect by the laser illumination is negligible, since the temperature dependence of the ac-photoconductance in Fig. 10 shows exactly the same trends as that

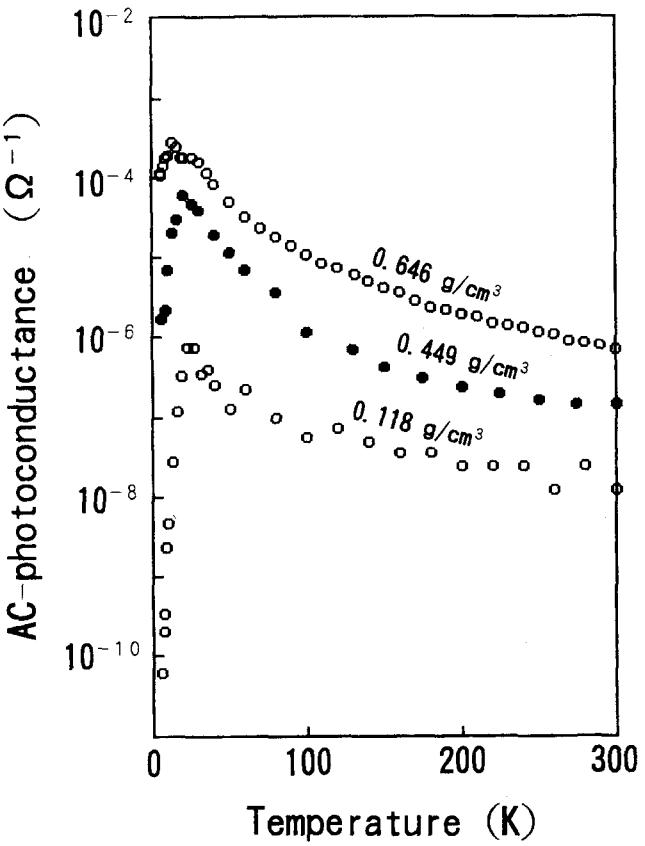

FIG. 10. The ac-photoconductance measured using an optical chopper and a lock-in-amplifier. The chopping frequency is 10 Hz and the duty cycle is 20%. The curves show the same trends as those of the dc-photoconductivity.

https://doi.org/10.1557/JMR.1993.0811 Published online by Cambridge University Press

of the dc-photoconductivity in Fig. 4. A quantitative comparison between these two results is difficult to make because the ac-photoconductance was measured with a two point electrode technique in order to have a good signal to noise ratio. Since the temperature dependence of the photoconductance differs so much from the least dense to the most dense carbon aerogel, this ac-photoconductance measurement is considered to be useful for the characterization of this kind of material. The chopping-frequency dependence of the ac-photoconductance is illustrated in Fig. 11 in log-log plots. In the low frequency range ($5 \leqq f \leqq 50$ Hz), the relation is linear and the slopes Δ are approximately the same (-0.80 to -0.84) for all three sample densities, as shown in the figure and summarized in Table III. Assuming a linear relation between the photoconductance and the photoconductivity, and using the relation $f = 0.2/t$, where t (s) and 0.2 are the pulse width and the duty cycle of the illumination, respectively, we obtain the following empirical equation for the photoconductivity $\Delta\sigma$:

$$\Delta\sigma = Ct^{0.8}. \tag{7}$$

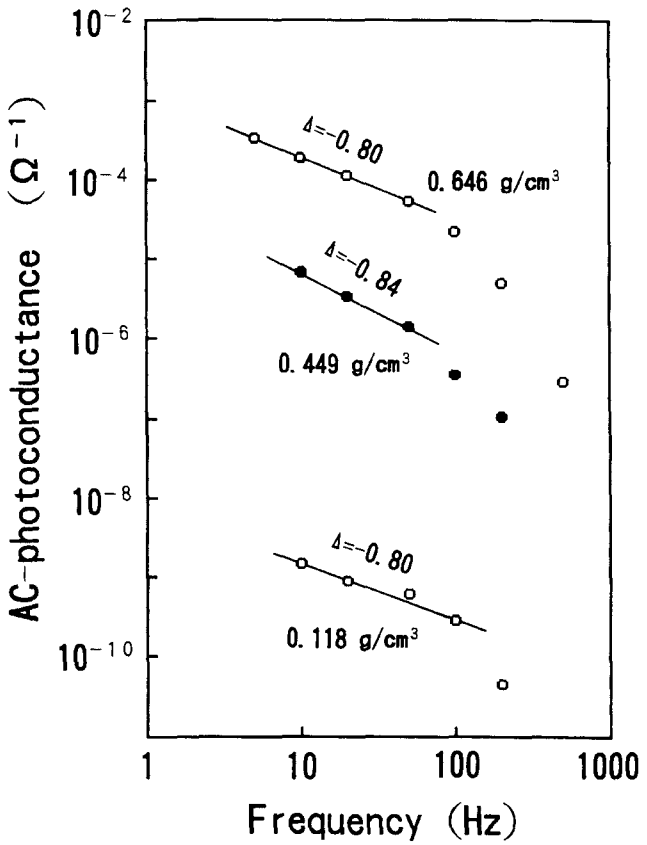

FIG. 11. The chopping-frequency dependence of the ac-photoconductance presented in log-log plots. In the frequency range 5–50 Hz, the relation is linear and the slopes Δ for the three samples are approximately the same (see text).

TABLE III. Values of the fitting parameters for the photoconductivity data.

Density (g/cm³)	0.118	0.449	0.646
E_r (meV)			
at high temp. ($T \geqq 100$ K)	22	25	22
at low temp. ($T \leqq 40$ K)	1.26	1.20	1.20
E_t (meV)	5.7	...	...
Δ*	−0.80	−0.84	−0.80

*Gradient for log f vs log (ac-photoconductance) in Fig. 11.

Here, C is a constant depending on the density of the carbon aerogel. This equation gives a rise time for the photoconductivity in the range $4 \times 10^{-3} \leqq t \leqq 4 \times 10^{-2}$ (s). The fact that the three samples have almost the same exponents (~0.8) in Eq. (7) indicates that the quantum efficiency values for the photocarrier generation in the particles are independent of the density, because the illuminating time period t in Eq. (7) is proportional to the incident photon number. In contrast, the term C in Eq. (7) is related to the interconnectivity of the particles because it depends on the density. In the frequency range over 50 Hz in Fig. 11, where $\Delta\sigma$ decreases with steeper gradient, the decreasing rates seem similar among the three samples, also indicative of the identity in the electronic structure of the particles.

IV. CONCLUSION

In the above discussion, we reach the conclusion that the photoconductivity measurements imply the existence of localized states, such as dangling bonds within the particles, although the dark conductivity is mainly limited by the fluctuation induced tunneling between the particles.

At high temperatures, the thermally activated dark carriers have a much larger population than the photoexcited carriers, and the photoconductivity is dominated by recombination. The activation energies for the recombinations are in the range 22–25 meV, and are almost independent of the density of the sample. This result indicates that there are recombination centers such as dangling bonds within each particle and the electronic structure of the particles is identical among the samples with different densities. The photoconductivity at low temperatures is dominated by the same carrier transport mechanism as that for the dark conductivity, because the activation energy values for the dark- and photoconductivities are similar. The population of the photocarriers is much larger than that of the dark carriers below ~20 K, especially in the lower density samples.

The qualitative characteristics of the photoconductivity in carbon aerogels are similar to those in a-Si and chalcogenides photoconductors, indicative of the existence of localized states in the mobility gap. The long decay times and the temperature dependence of the

https://doi.org/10.1557/JMR.1993.0811 Published online by Cambridge University Press

activation energy for the recombination can be explained by a relaxation process involving the dangling bonds.

ACKNOWLEDGMENTS

We are thankful to Dr. G. Dresselhaus, Dr. S. L. di Vittorio, Dr. Z. H. Wang, A. W. Fung, and J. J. Chen for enlightening discussions and help with the experiments. We gratefully acknowledge support from Lawrence Livermore National Laboratory Subcontract No. B130530 and from the Toshiba Corporation. The aerogel synthesis was performed under the auspices of the United States Department of Energy by Lawrence Livermore National Laboratory under Contract No. W-7405-ENG-48.

REFERENCES

1. J. Steinbeck, G. Braunstein, M. S. Dresselhaus, G. Dresselhaus, and T. Venkatesan, in Extended Abstracts No. 8 (*Graphite Intercalation Compounds*), edited by M. S. Dresselhaus, G. Dresselhaus, and S. A. Solin (Materials Research Society, Pittsburgh, PA, 1986), p. 129.
2. J. M. MacFarlane, I. S. McLintock, and J. C. Orr, Phys. Status Solidi A **3**, K239 (1970).
3. B. D. McMichael, E. A. Kmetko, and S. Mrozowski, J. Opt. Soc. Am. **44**, 26 (1954).
4. K. Kuriyama and M. S. Dresselhaus, J. Mater. Res. **6**, 1040 (1991).
5. K. Kuriyama and M. S. Dresselhaus, Phys. Rev. B **44**, 8256 (1991).
6. R. W. Pekala and F. M. Kong, Polym. Prpts. **30**, 221 (1989).
7. R. W. Pekala and F. M. Kong, J. Phys. (Paris) Coll. Suppl. **50**, C4-33 (1989).
8. R. W. Pekala and C. T. Alviso, in *Novel Forms of Carbon,* Mater. Res. Soc. Symp. Proc. (1992, in press).
9. R. W. Pekala, J. Mater. Sci. **24**, 3221 (1989).
10. R. W. Pekala, C. T. Alviso, and J. D. LeMay, in *Chemical Processing of Advanced Materials,* edited by L. L. Hench and J. K. West (John Wiley & Sons, Inc., New York, 1992), pp. 671–683.
11. R. W. Pekala, C. T. Alviso, F. M. Kong, and S. S. Hulsey, J. Non-Cryst. Solids **145**, 90 (1992).
12. A. W. P. Fung, Z. H. Wang, K. Lu, M. S. Dresselhaus, and R. W. Pekala, unpublished work.
13. P. Sheng, E. K. Sichel, and J. I. Gittleman, Phys. Rev. Lett. **40**, 1197 (1978).
14. J. Mort and D. M. Pai, *Photoconductivity and Related Phenomena* (Elsevier Scientific Publishing Co., Amsterdam, 1976), pp. 195, 241.
15. W. E. Spear, R. J. Loveland, and A. Al-Sharbaty, J. Non-Cryst. Solids **15**, 410 (1974).
16. T. C. Arnoldussen, C. A. Menezes, Y. Nakagawa, and R. H. Bube, Phys. Rev. B **9**, 3377 (1974).
17. D. V. Lang and R. A. Logan, Phys. Rev. Lett. **39**, 635 (1977).
18. D. V. Lang, R. A. Logan, and M. Jaros, Phys. Rev. B **19**, 1015 (1979).
19. S. C. Agarwal and S. Guha, Phys. Rev. B **31**, 5547 (1985).
20. J. Kakalios and H. Fritzsche, Phys. Rev. Lett. **53**, 1602 (1984).
21. R. H. Bube, *Photoconductivity of Solids* (John Wiley, New York, 1960).
22. M. H. Brodsky, *Amorphous Semiconductors* (Springer-Verlag, 1985), p. 139.
23. A. Rose, *Concepts in Photoconductivity and Allied Problems* (Interscience Publishers, New York, 1963).
24. F. Stöckmann, in *Proceedings of the Third International Conference on Photoconductivity* (Pergamon Press, New York, 1971), p. 17.

https://doi.org/10.1557/JMR.1993.0811 Published online by Cambridge University Press